









Historical dynamics of landslide risk from population and forest-cover changes in the Kivu Rift

Arthur Depicker¹  , Liesbet Jacobs¹, Nicholus Mboga², Benoît Smets^{3,4} , Anton Van Rompaey¹, Moritz Lennert², Eléonore Wolff², François Kervyn³, Caroline Michellier³, Olivier Dewitte³   and Gerard Govers¹ 

Human activity influences both the occurrence and impact of landslides in mountainous environments. Population pressure and the associated land-use changes are assumed to exacerbate landslide risk, yet there is a lack of statistical evidence to support this claim, especially in the Global South where historical records are scarce. In this work, we explore the interactions between population, deforestation and landslide risk in the Kivu Rift in Africa. To do so, we develop a holistic landslide risk model that evaluates 58 years of population and forest-cover trends. We show that the current landslide risk in the eastern Democratic Republic of the Congo (DRC) is twice as high as in neighbouring Rwanda and Burundi. Congolese households, on average, populate more hazardous terrain, probably as a result of conflicts and economic pull factors such as mining. Moreover, the recent large-scale deforestation of primary rainforest in the DRC has considerably exacerbated the landslide risk. Our analysis demonstrates how the legacy of deforestation, conflicts and population dynamics is reflected in the landslide risk in the Kivu Rift.

Disaster risk reduction is inextricably connected to sustainable development^{1,2}. Between 1975 and 2015, the global population increased from 4 to 7 billion people³ and simultaneously the number of people exposed to natural hazards nearly doubled⁴. The growing demand for food and resources, as well as the loss of soil productivity due to poor land management, have incited people to expand agricultural land at the expense of near-natural ecosystems^{5–7}. In hilly and mountainous areas, this agricultural expansion frequently increases landslide risk as population expansion can be associated with settlements in steeper terrain⁸. The environmental degradation processes associated with land settlement can, in turn, increase landslide hazard^{9,10}. Quantifying these human–nature interactions is thus a prerequisite to understand the occurrence of landslides, as well as the risk they pose to humans. The latter is substantial, causing thousands of fatalities every year^{11,12}.

Since the 1970s, scientists have addressed the question of ‘where’ landslides are likely to occur by means of susceptibility assessments¹³. However, these analyses fall short in addressing a number of key questions that need to be answered to fully grasp the interactions between environment, landslides and humans. For example, susceptibility assessments do not explicitly quantify the frequency and size of landslides (the hazard), nor do they consider the actual risk posed to livelihoods, namely the expected number of casualties and economic damage^{14,15}. Also, the vast majority of studies have considered landslide susceptibility to be static in time¹³. Recent evidence advocates for a more dynamic approach whereby susceptibility is allowed to vary over time, reflecting changes in the environment^{16–18}.

Deforestation is one of the key environmental changes to affect landslide hazard¹⁰. The rapid transition from forests into cultivated or bare land is associated with a surge in shallow landsliding that can persist for more than a decade^{10,19,20}. Many authors make

an argument for forest conservation by supposing a link between deforestation-induced landsliding and a growing risk posed to society^{21,22}, but there is a lack of quantitative evidence to support this assumption^{23–25}. Investigating these human–nature interactions is challenging, especially in the Global South, due to the scarcity of detailed landslide and forest-cover records^{26,27}.

In this study, we investigate how landslide risk trends in the Kivu Rift (Fig. 1) have been affected by population pressure and forest-cover changes during the past six decades. The Kivu Rift is embedded in the western branch of the East African Rift, where tectonic uplift has produced mountain ranges that have been identified as a global hotspot of landslide risk^{28–31}. The area encompasses Lake Kivu and parts of its three surrounding countries: Burundi, the Democratic Republic of the Congo (DRC) and Rwanda. Landslide casualties are frequent with about 50 fatalities reported annually between 2016 and 2018 for Rwanda alone, though the actual number is likely to be higher^{27,32}. Tropical forest, the dominant vegetation along the Rift shoulders before the twentieth century, only persists in a few protected areas in Rwanda and Burundi^{33,34}. Meanwhile, the forest in the Congo Basin was, until recently, largely preserved^{33,35,36}. In recent decades, rapid population growth in the eastern DRC, which was also due to a large influx of Rwandan refugees in 1994, has probably led to an increased pressure on the remaining forest area^{3,37,38}. To this day, the management and conservation of forests in the DRC is hampered by political instability^{39,40}. Thus, historically, the timing of deforestation has varied widely between the different countries in the Kivu Rift³³. Moreover, deforestation as a driver of changing landslide activity is expected to exceed the importance of other drivers such as climate change^{12,41}, especially in the Kivu Rift where evidence for any past decadal trends in extreme precipitation remains feeble^{12,43}. The study area is therefore an ideal setting to investigate how population pressure affects landslide risk resulting

¹Department of Earth and Environmental Sciences, Division of Geography and Tourism, KU Leuven, Heverlee, Belgium. ²Department of Geosciences, Environment & Society, Université Libre de Bruxelles, Brussels, Belgium. ³Department of Earth Sciences, Royal Museum for Central Africa, Tervuren, Belgium. ⁴Department of Geography, Cartography and GIS Research Group, Vrije Universiteit Brussel, Brussels, Belgium.

✉e-mail: arthur.depicker@kuleuven.be; olivier.dewitte@africamuseum.be

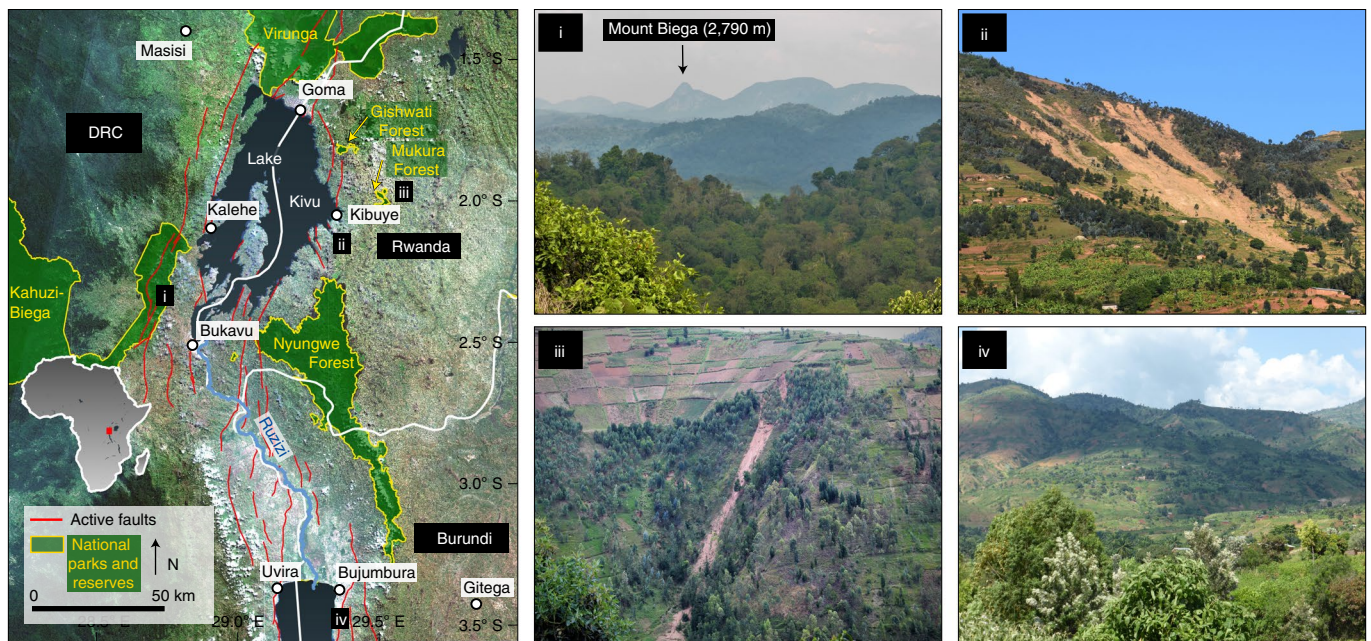


Fig. 1 | Overview of the Kivu Rift. The map illustrates the active faults that cause rifting and tectonic uplift²⁸, and the protected areas (reserves and parks). A Sentinel-2 image composite is used as a background layer⁶⁵. Photo locations: (i) tropical forest in Kahuzi-Biega National Park (28.7470° E, 2.3344° S); (ii) rainfall-induced landslide event in Karongi District, Rwanda, inflicting approximately 20 fatalities on the evening of 6 May 2018 (29.3674° E, 2.1491° S); (iii) a shallow debris slide in Rwanda (29.5884° E, 1.9674° S); and (iv) strongly anthropized landscape in Burundi; the original forest cover was removed prior to 1958 (29.3631° E, 3.4764° S).

from deforestation and settlement expansion, and how this can be managed more sustainably.

We use historical, panchromatic aerial photographs and regional land-cover maps to reconstruct the annual forest dynamics in the Kivu Rift and we apply these data to model the multidecadal dynamics of landslide susceptibility, hazard and risk. We use nearly 2,400 photographs from 1958 to construct an orthomosaic that reveals the forest cover in the study area (the ‘Forest cover in 1958’ section in the Methods). We combine this historical forest map with more recent regional land-cover products (the ‘Forest cover in 1988, 2001 and 2016’ section in the Methods) to recreate the annual forest-cover changes between 1958 and 2016 (the ‘Annual forest-cover changes’ section in the Methods). Subsequently, we use an existing landslide inventory to (1) develop a dynamic landslide susceptibility model that responds to forest-cover changes and (2) calibrate the relationship between susceptibility and hazard. As such, the annual forest data allow us to assess the evolution of the landslide hazard (the ‘Landslide hazard and forest-cover changes’ section in the Methods). Finally, the annual landslide hazard is combined with the distribution of the population density at different points in time to quantify historical trends in landslide risk (the ‘Landslide hazard and forest-cover changes’ section in the Methods).

The Kivu Rift in 1958

Most of the forests in Rwanda and Burundi had already been converted into agricultural land by 1958, with the remaining forests covering ~19% and ~29% of the total land surface area, respectively (Fig. 2). Large-scale deforestation had been necessary to sustain the at-the-time already large population in Rwanda and Burundi (on average 94 inhabitants per km² in 1958) and to remediate recurrent food crises⁴⁴. In the eastern DRC, population pressure was much smaller, as the average density in the wider Kivu region was estimated at only 17 inhabitants per km² in 1958 (refs. ^{3,45}). As a result, forests still covered 70% of the countryside in the DRC west of Lake Kivu in 1958.

In 1958, the forests in our study area were much less accessible than nowadays³⁵ (the ‘Annual forest-cover changes’ section in the Methods). The built-up area in the entire Kivu Rift increased by a factor of 2.5 between 1958 and 2016, while population increased by a factor of 5 in the same period.^{3,44} Thus, population density within built-up land more or less doubled between 1958 and 2016 (ref. ⁴⁶). The road network was less dynamic, with 87% of the road length mapped in 2016 already existing in 1958. However, the relatively modest expansion of the network in the DRC unlocked relatively large portions of previously inaccessible forest (Supplementary Fig. 1). The development of infrastructure is often associated with mining or timber concessions and is therefore expected to have accelerated deforestation³⁶.

Forest and societal dynamics (1958–2016)

Forest-cover changes in the Kivu Rift are highly variable in space and time (Fig. 3). Between 1958 and 1988, the deforestation rates in the Kivu Rift generally remained low, despite a tripling of the population in Rwanda and Burundi and a sixfold increase in the DRC (Fig. 3b). The forest-cover loss became more substantial at the time when conflicts emerged in the region^{39,40,47,48} (Fig. 3a,b). In October 1990, a civil war erupted in Rwanda, protracting until August 1993 and followed by the genocide against the Tutsi between April and July 1994. This period of conflict initiated the relocation of 2 million refugees, half of which fled to the Kivu region in the eastern DRC^{47,49}. Within Rwanda, displaced people settled in the highlands ~10 km east of Gisenyi and Goma, clearing and fragmenting the Gishwati Forest to satisfy their need for food and fuelwood (Fig. 3c)^{47,48}. We estimate that since 1958, more than 80% of the Gishwati Forest has been converted to pasture land. Due to these developments, there was a substantial forest decline in Rwanda between 1988 and 2001 (Fig. 3b). During the same period in Burundi, where a civil war started in 1993, the forests shrunk at a rate of 1.6% per year (Fig. 3b). The conflict in Burundi ceased in 2005 (Fig. 3a). In recent decades, the governments

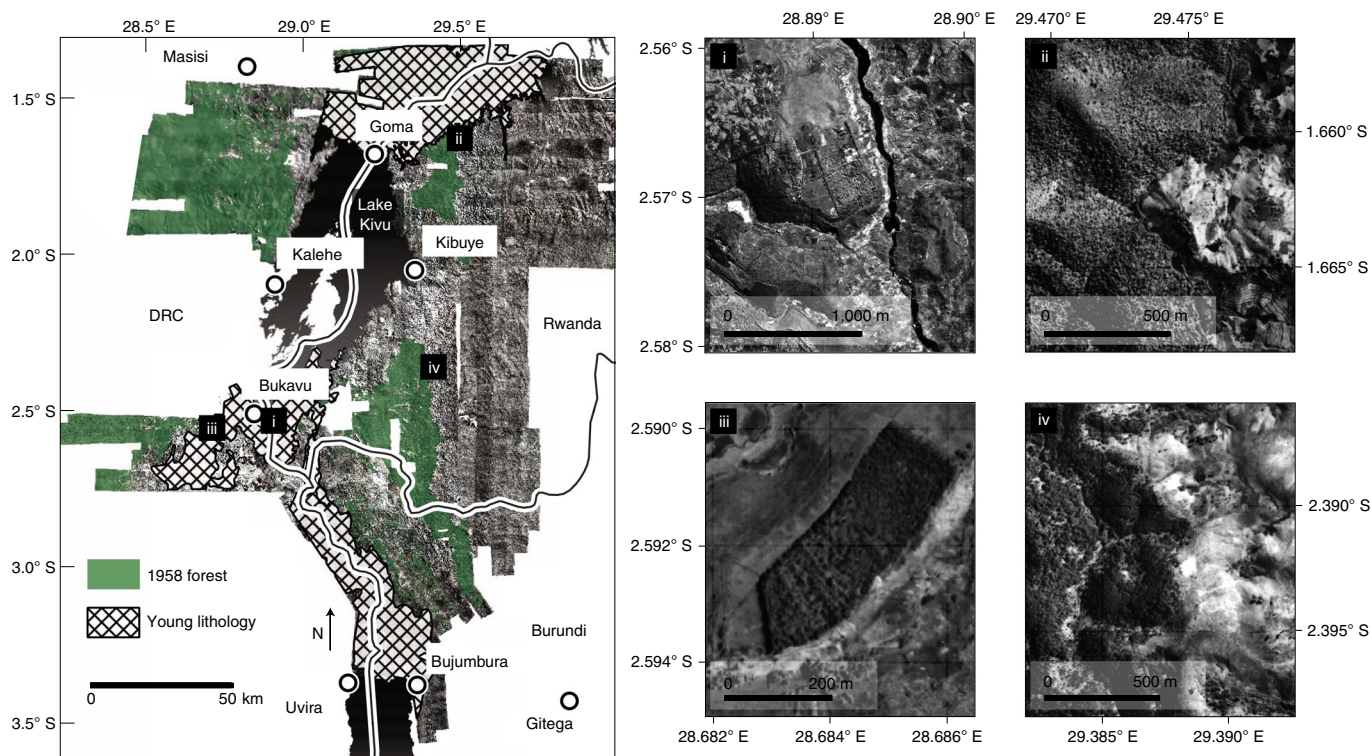


Fig. 2 | The 1958 orthomosaic and forest cover for the Kivu Rift. Locations on the map: (i) Ruzizi River near Bukavu (28.8914° E, 2.5687° S); (ii) eastern edge of Gishwati Forest (29.4750° E, 1.6627° S); (iii) planted forest west of Bukavu (28.6844° E, 2.5919° S); and (iv) eastern edge of Nyungwe Forest (29.3879° E, 2.3925° S). Our study area is confined by the extent of the historical photographs and excludes areas of young lithology (volcanic rocks and river and lake sediments; more details in the ‘Forest cover in 1958’ section in the Methods).

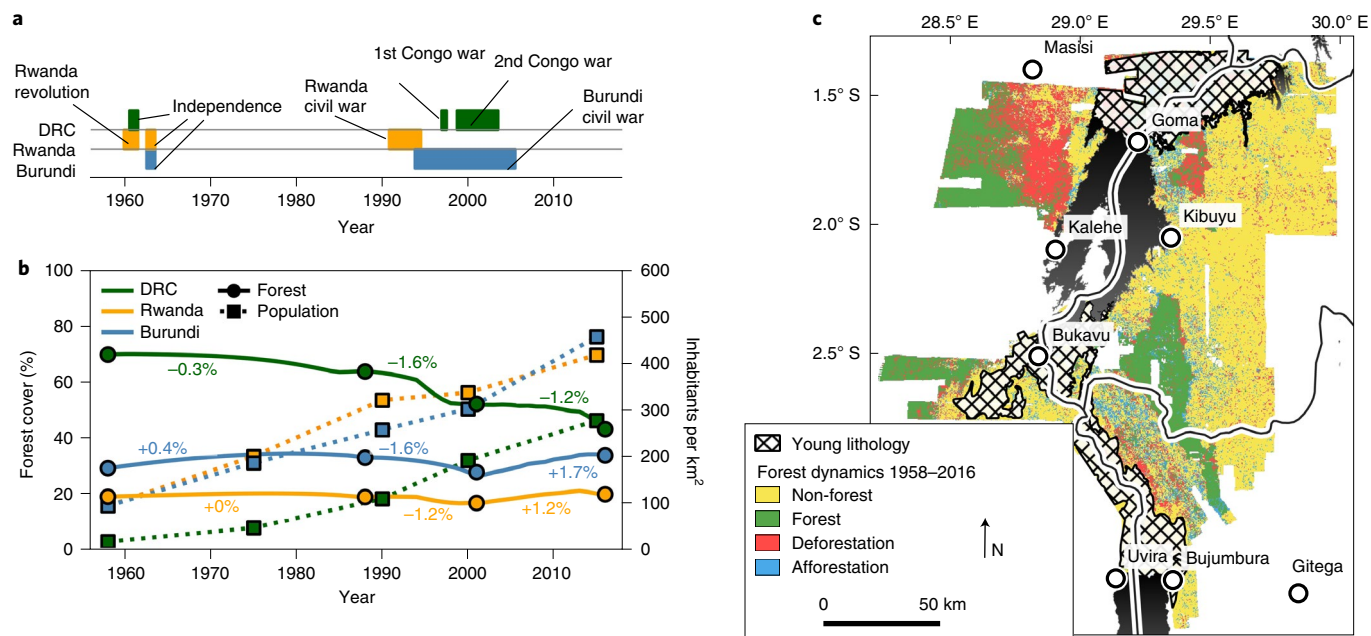


Fig. 3 | Conflicts, forest dynamics and demography in the Kivu Rift. **a**, Timeline of the major conflicts in the Kivu Rift. **b**, The forest-cover and population trends⁴⁶. The values indicate the mean annual forest-cover change. The annual forest-cover changes between four observations (1958, 1988, 2001 and 2016) are reconstructed by means of annual change estimates (how much land is deforested and afforested every year?) and deforestation and afforestation likelihood models (where will deforestation/afforestation happen first?; ‘Annual forest-cover changes’ section in the Methods). **c**, Forest-cover dynamics between 1958 and 2016. Source data

of Rwanda and Burundi have implemented various afforestation schemes^{50,51}, leading to an average annual increase in forest cover (Fig. 3b).

The fallout of the conflict in Rwanda disrupted the environmental and political landscape of the eastern DRC^{39,40}. Soon after the influx of Rwandan refugees in 1994, the First Congo War erupted

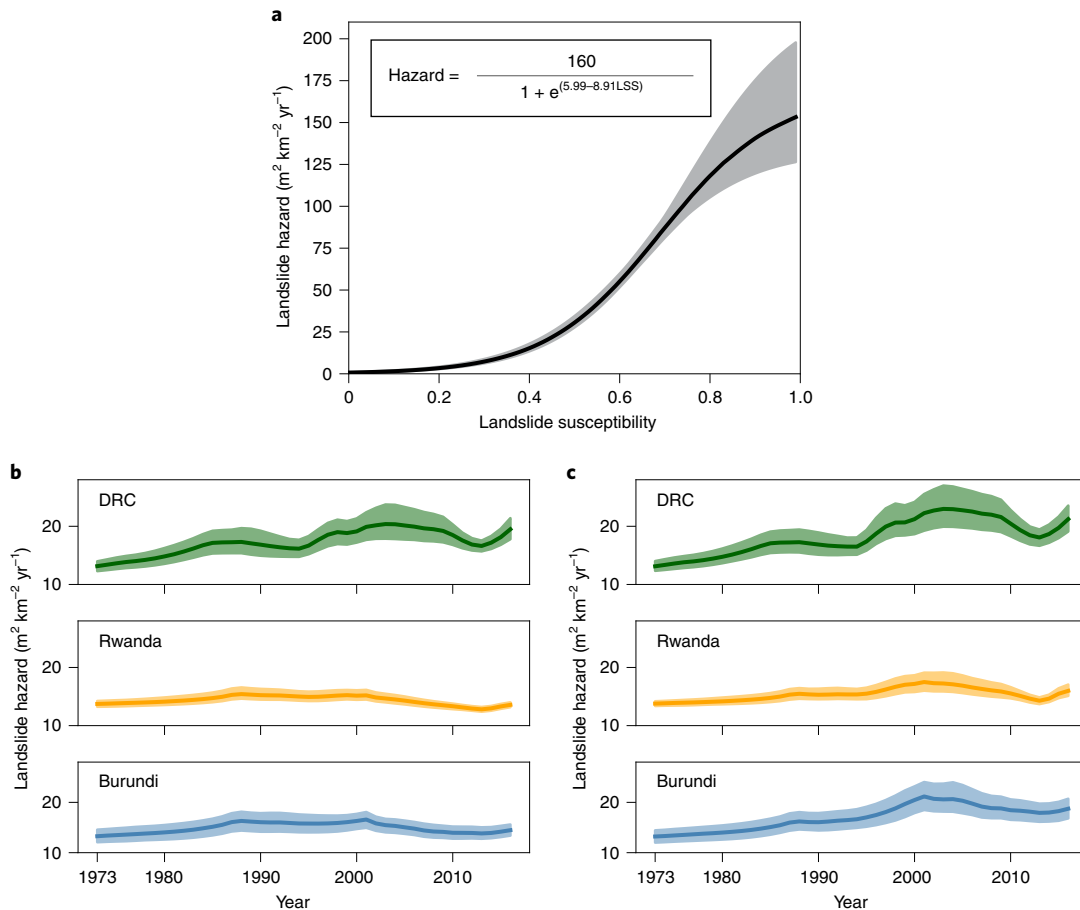


Fig. 4 | Landslide hazard trends in the Kivu Rift and the link with landslide susceptibility. **a**, Nonlinear relationship between landslide susceptibility and landslide hazard. **b**, Landslide hazard trends in the Kivu Rift when we assume the landslide response to deforestation is the same for new and primary forests. **c**, Landslide hazard trends when we assume there is no landslide response to deforestation in new forests. The solid lines in all panels indicate the median landslide hazard estimates, while the shaded areas indicate the 80% confidence intervals, which are calculated by applying Efron's bootstrap to the susceptibility model ('Landslide hazard and forest-cover changes' section in the Methods). Source data

(November 1996–May 1997), almost immediately followed by the Second Congo War (August 1998–July 2003)⁵². These conflicts and the related issues with refugees and internally displaced people were a major factor in the doubling of population density from 109 to 192 inhabitants per km² between 1990 and 2000 (ref. ⁴⁶) (Fig. 3a,b). Simultaneously, the international demand for gold and 3T minerals (tin, tantalum and tungsten), commodities abundantly present in the eastern DRC, grew considerably^{53–55}. In response, mining activity in the region increased rapidly^{56,57}. The development of mining sites had a low direct impact on the forest cover⁵⁸, but the associated construction of roads and settlements facilitated access to the primary forest, making it more vulnerable to smallholder clearing and fuelwood extraction³⁶. The influx of refugees and internally displaced people, combined with the growing mining industry, coincided with a strong forest decline during the 1990s that has persisted even after 2001 (Fig. 3a,b).

In all three countries deforestation happened primarily close to roads and along the edges of forests, which is in line with previous observations that the population pressure on forest resources is more pronounced in locations that are easily accessible^{35,36} (Supplementary Table 1). Generally, natural parks and reserves experienced less deforestation, showing that a protection status has a positive effect on conservation⁴⁰. However, the effect was smaller in the DRC, especially in the most recent years (Supplementary Table 1). The role of slope gradient in deforestation is ambiguous (Supplementary Table 1):

from 1958 to 1988, deforestation tended towards gentler slopes, while between 1988 and 2016 the opposite was true in Rwanda and Burundi. This result may be explained by the fact that households in Rwanda and Burundi largely relied on planted forests for their wood supply. Indeed, roughly half of the deforestation in Rwanda and Burundi occurred in 'new' forests that emerged on steeper terrain after 1958 (Supplementary Table 1). We assume that most of these 'new' forests were planted given that afforestation mainly happened away from the forest edges (Supplementary Table 2), making natural regeneration highly unlikely⁵⁹.

Impact of forest-cover changes on landslide hazard

Our calibrated landslide susceptibility model estimates that deforestation increases the odds of landsliding temporarily by a factor of 10 to 28, depending on the geomorphic context. Likewise, afforestation decreases the odds of landsliding by a factor of 1.5 to 4. The model discriminates between landslide and non-landslide locations with an accuracy of 89%, an improvement of 6% compared with previously developed susceptibility models for the study area where forest cover was considered static²⁹.

In our baseline scenario, we assume that the cutting of new forests (planted or naturally regenerated) does not incite a landslide response (Fig. 4b). This scenario is in line with previous research suggesting that the first deforestation-induced landslide wave alters the slope properties by depleting the most landslide-sensitive slope

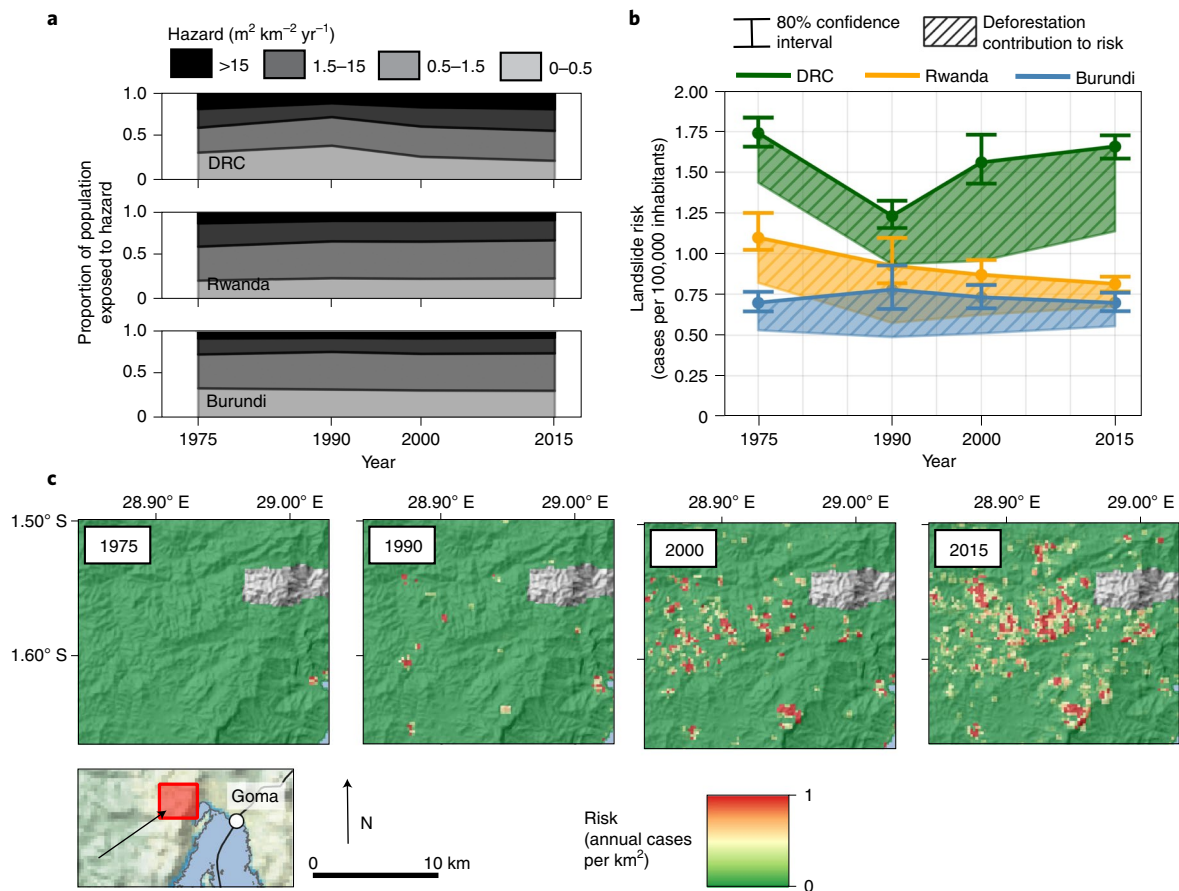


Fig. 5 | Landslide exposure and risk in the Kivu Rift. **a**, Exposure of the population to landslide hazard. **b**, Landslide risk trends and the impact of deforestation. **c**, Spatially explicit landslide risk assessment in four periods south of Masisi and west of Goma. For these risk maps, we presented the risk in a spatially explicit way (the number of cases per km² per year) and improved the visual representation by decreasing the raster resolution by a factor of 10, retaining the maximal value of aggregated pixels. The average risk in this location in 2015 is 5.7 cases per 100,000 inhabitants, more than three times higher than the average risk in the studied part of the DRC (Supplementary Fig. 4). Source data

material, thus reducing the long-term landslide occurrence regardless of future forest-cover changes²⁰. If, on the contrary, new forests responded in the same way to deforestation as primary forests (Fig. 4c), the estimated landslide hazard (affected area per km² yr⁻¹) in the DRC, Rwanda and Burundi would be, on average, 3.9%, 5.7% and 10.5% higher, respectively.

In all three countries, the hazard increases with time until a peak is reached around 2001 (Fig. 4b,c). Our model shows that the cumulative effects of forest-cover changes since 1958 resulted in a net hazard increase of 81–103% in the DRC, 10–27% in Rwanda and 21–58% in Burundi. In all three countries, hazard initially decreases after 2001, a trend that is related to the reduction of deforestation rates. In the DRC, the landslide hazard rises again after 2013 (Fig. 4b,c), due to a strong increase in net deforestation (Fig. 3b).

Impact of deforestation and growing exposure on landslide risk

Landslides in uninhabited regions do not have the same societal impact as landslides in a densely populated area. We observe that, within the DRC, a larger proportion of the population is located on terrain with a high landslide hazard, especially after 1990 (Fig. 5a). In Burundi and Rwanda, the population generally resides in less hazardous terrain. Moreover, no changes in exposure for Burundi and Rwanda are apparent between 1975 and 2015.

We recognize that we only look at one aspect of risk (the expected number of fatalities, Fig. 5b). Moreover, we only account

for the exposure of the population and not its vulnerability, which is defined as the mortality probability of a person in case of a landslide encounter⁶⁰. While data on vulnerability are not available for our study area, we can assume it to be high, given the limited economic development in the region (the ‘Risk based on hazard and exposure’ section in the Methods)⁶⁰. In addition, the calculated hazard may be an underestimation of the real hazard due to the potential omission of landslide events in our landslide inventory. Therefore, the reported risk is a means to compare the relative landslide risk context between different regions and/or periods, rather than to make an accurate estimation of the expected number of landslide victims.

The landslide risk is consistently higher in the DRC when compared with its neighbouring countries (Fig. 5b). While overall risk displays a slightly decreasing trend in Rwanda and Burundi, the temporal variability is larger in the DRC. Here, the initial risk in 1975 is high due to the concentration of a small population along the steep northwestern shores of Lake Kivu. Up to the 1990s a sharp decrease in risk is visible, but afterwards the risk peaks again, simultaneously with the hazard (Fig. 4b). In 2015, the risk in the DRC is roughly twice as large as in Rwanda and Burundi. Even when assuming that the removal of new forests results in the same landslide response as the cutting of primary forests, these relative differences in risk persist (Supplementary Fig. 2). Between 2000 and 2015, forest-cover changes increased the shallow landslide risk in the DRC by 55%, compared with 30% and 34% in Rwanda and Burundi, respectively (Fig. 5b; the ‘Risk based on hazard and

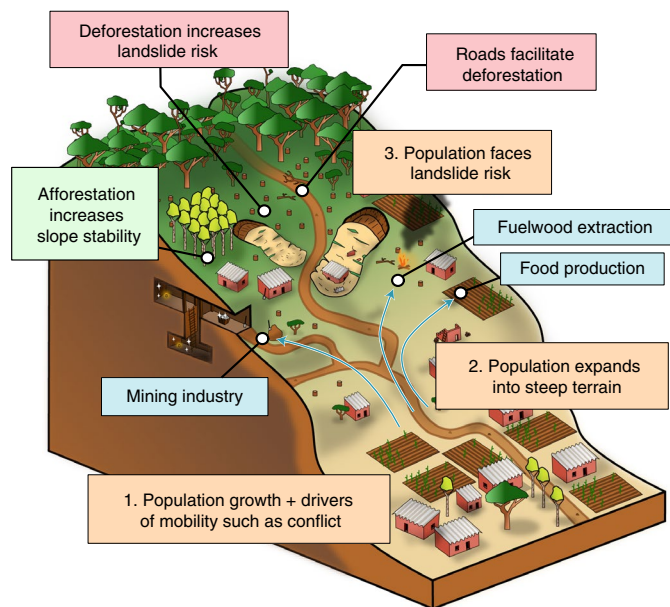


Fig. 6 | Conceptual overview of the key processes affecting shallow landslide risk in the Kivu Rift. The orange boxes represent the trajectory of the population. The blue boxes show the pull factors that attract people to steep terrain. The red boxes indicate human disturbances that directly or indirectly exacerbate the landslide risk, while the green box represents interactions that reduce the landslide risk.

exposure' section in the Methods). The effects of forest-cover changes are not sufficient to explain the higher risk in the DRC: an important fraction of the Congolese population is located on terrains that are steeper (Supplementary Fig. 3) and thus more susceptible and hazardous (Fig. 5a).

Shallow landslide risk is spatially very heterogeneous, with most areas displaying little to no risk and a few areas that display a very high risk (Supplementary Fig. 4). Within the DRC, the risk hotspot between 2000 and 2015 is situated in the rural territories located south of Masisi and west of Goma (Fig. 5c). While the overall risk in the DRC within our study area is 1.7 cases per 100,000 inhabitants per year, the average risk in this particular region is roughly 5.7 cases per 100,000 inhabitants per year, that is, more than three times higher.

Discussion

We present statistical evidence that population pressure and the associated deforestation have led to an increased landslide risk in the Kivu Rift. We find that the contemporary landslide risk in the eastern DRC is at least twice as high as in Rwanda and Burundi. The large differences in overall landslide risk are only partly due to the poor protection of forest resources in the DRC (Fig. 5b). Even in a hypothetical scenario where deforestation is absent, the risk in the DRC would still be at least 69% higher compared with its neighbouring countries. The remaining risk gap with Rwanda and Burundi is explained by the location of Congolese households on more hazardous, generally steeper terrain (Supplementary Fig. 3). This is a result from the important population growth in the countryside of the eastern DRC, leading to a sprawl of settlements and the associated subsistence farming in hilly terrain (Fig. 6)³⁷.

Besides natural population growth due to high birth rates, this demographic evolution can be linked to two other major factors. The first is conflict: the relocation of hundreds of thousands of Rwandan refugees in 1994 and the internal displacement of people during and following the First and Second Congo wars^{37,56,61}. The second factor is the expanding artisanal and industrial mining

industry, fuelled by a globally increasing demand for gold and 3T minerals^{53–55}. This economic opportunity has incited a large number of people to settle in the mineral-rich hinterland of Lake Kivu, for example, Masisi and its southern satellite towns^{55,56}. The issues of refugees, internal displacement and mining are of less importance within Rwanda and Burundi⁶².

Our model shows a large spatial and temporal variation in landslide risk that is highly influenced by forest cover, demographic shifts and settlement patterns (Fig. 4b,c). The risk at a local level may be up to three times higher than the average risk at a regional scale (Fig. 5c). Generally, such a high local risk is related to the expansion of a rural population in steep terrain at the expense of forests (Fig. 6). Landslide risk can in principle be reduced by setting up policies to raise awareness and understanding of the problem²⁶, both in farming and mining communities. However, it is even more important to reduce the incentives for the local population to settle in hazardous areas as it influences both hazard (through deforestation) and risk (through increased exposure). This goal can be achieved by, for instance, encouraging the use of permanent agricultural land in low-hazard areas instead of slash and burn agriculture^{63,64}. Such a policy requires investments to increase the productivity of croplands⁶³. The extraction of fuelwood (and hence deforestation) from primary forest can also be reduced by using more efficient stoves and/or by replacing fuelwood with other energy sources where this is feasible⁵⁰. At the same time, forests planted in hazardous areas may not only reduce landslide risk but may also serve as a source of fuelwood⁵⁰. All these policies would reduce the loss of primary forest and can facilitate reforestation, thereby initiating a forest transition.

Our analysis demonstrates the complexity of interactions between shallow landslide hazard and forest dynamics, indicating that a regional assessment solely based on a direct causal linkage between net forest-cover change and landslide hazard would be incomplete. Thus, to assess the evolution of landslide risk, we show that it is important to apply a spatially explicit approach and to account for the legacy of environmental and societal changes over a multidecadal timespan. Considering our observation that deforestation, compared with afforestation, exerts a larger effect on susceptibility and thus hazard, even a net expansion of forest cover can be associated with an increase in landslide hazard. It is pivotal to account for the spatial patterns in deforestation to estimate its overall impact on hazard, as the absolute impact of deforestation depends on the preexisting susceptibility conditions. Furthermore, the impact of deforestation on hazard is temporary, and knowledge of the timing of forest-cover changes is also essential to assess the temporal dynamics of the landslide hazard.

While our study focused on the past, some of the drivers we identified (deforestation, mining activity and population expansion in steep terrain; Fig. 6) are expected to be of high relevance for the future development of the area, especially in the highlands of the Kivu region in the eastern DRC^{55–58}. Local and national governments as well as organisations that are locally active should therefore account for these drivers when designing disaster-risk-reduction programs related to the region.

Methods

Forest cover in 1958. We use the historical, panchromatic aerial photographs from 1958 conserved at the Royal Museum for Central Africa in Belgium to capture the forest cover in the Kivu Rift (<http://pastecca.africamuseum.be/>). In a first step, we use photogrammetric techniques to create a georeferenced and orthorectified mosaic (henceforth called orthomosaic) with a spatial resolution of ~1 m, and subsequently convert this panchromatic image into forest cover by means of object-based classification techniques. As such, we obtain a 1958 forest-cover map with an accuracy of 96.7% (Supplementary Methods). Our study area within the Kivu rift is thus limited by the extent of the orthomosaic. Moreover, interactions between forest cover, deforestation and landslides are only well understood in older lithology²⁰. Hence, we exclude areas of younger lithology (for example, from volcanic origin or sediments) from our subsequent analysis. The major urban centres in the Kivu Rift (Goma, Bukavu and Bujumbura) are located within areas

of younger lithology and are therefore also excluded. Our study area could thus be considered as the 'countryside' of the Kivu Rift (Fig. 2).

Forest cover in 1988, 2001 and 2016. Besides the historical photographs, we have access to a range of regional and continental datasets to assess historical forest coverage. We use the regional land-cover maps for 1988 and 2001 provided by Basnet and Vodacek⁶⁶. These maps are provided at a 30 m resolution and were derived from Landsat imagery. The overall accuracy of the maps is reported to be at least 90% (ref. ⁶⁶). We reclassified the land-cover maps into forest-cover maps by merging the following land-cover classes: (1) 'forest' and (2) 'open/degraded forest'. The 2016 forest cover is extracted from the continental European Space Agency Climate Change Initiative (ESA-CCI) prototype land-cover model, provided at a 20 m resolution and derived from Sentinel observations⁶⁷. Contrary to the regional land-cover maps from Basnet and Vodacek⁶⁶, the accuracy of the ESA-CCI model within the Kivu Rift is unknown. We assess the accuracy of its 'forest' land-cover class by validating 500 forest and 500 non-forest points. These points are randomly sampled in areas where Google Earth has imagery available for the year 2016, so that these 1,000 points can be validated for the correct time period. We estimate the 95% confidence interval of the accuracy by recalculating it 1,000 times, each time sampling 500 forest and 500 non-forest points (with replacement) from our validation dataset. As such, we observe an accuracy of $86.1 \pm 2.1\%$.

Annual forest-cover changes. To reconstruct the annual forest-cover changes in between our four distinct forest-cover observations (1958, 1988, 2001 and 2016), we develop a new spatially explicit forest-dynamics model following the approach of He et al.⁶⁸ and Bolliger et al.⁶⁹. Our forest-dynamics model integrates four major components: (1) a deforestation likelihood model, (2) an afforestation likelihood model, (3) an annual deforestation rate estimate N_{def} and (4) an annual afforestation rate estimate N_{aff} . For every year between 1958 and 2016 we recalculate the deforestation and afforestation likelihoods and remove/add the $N_{\text{def}}/N_{\text{aff}}$ forest pixels with the highest predicted likelihood. We use the STATSMODELS and GDAL packages in Python 3.5 (<https://www.anaconda.com/>) to implement the forest-dynamics model and import and export the spatial data (idem for the 'Landslide hazard and forest-cover changes' and 'Risk based on hazard and exposure' sections).

The binary outcome of our dependent variable (deforested versus conserved) is modelled through logistic regression⁷⁰. The basic equation of logistic regression is:

$$\log\left(\frac{P}{1-P}\right) = \alpha + \sum_{i=1}^n \beta_i X_i, \quad (1)$$

with P the likelihood of deforestation, α the intercept, X_i the i th of n predictors and its accompanying coefficient β_i .

The dependent variable is derived from annual deforestation data that are obtained from global forest-cover-change data provided for the period 2001–2017 (ref. ⁷¹). To ensure the accuracy of these training data, we only retain the data that can be validated with the more accurate 2001 regional and 2016 continental forest data^{66,67}. For example, when the global data indicate a pixel that has been deforested, we only retain this pixel as deforested when the 2001 regional data indicate forest and the 2016 continental data indicate no forest. Note that we potentially exclude areas that are deforested and subsequently afforested again between 2001 and 2016. However, due to the lack of annual afforestation data, the identification of such locations is not possible. In total, we retained 91% of the non-forest area presented by the global model⁷¹, 86% of the forest area and 34% of the deforested areas to sample training data for the deforestation likelihood model. In total, we sample 3,500 deforestation points (equally spread over the different years) and 3,500 conservation points from these 'validated' global forest data.

Within our likelihood model we incorporate a number of predictors that were selected in agreement with existing deforestation modelling literature^{69,72,73}. We included (1) protection status (0/1), that is, whether or not the area is part of a park or reserve; (2) the forest edge^{69,73} (0/1), indicating the presence of neighbouring non-forest pixels and (3) deforestation contagion⁷² (0/1), defined as the presence of neighbouring pixels that were deforested in the previous year. Moreover, we incorporate three predictors derived from the one arcsecond resolution Shuttle Radar Topography Mission digital elevation model: (4) elevation (m), (5) slope (degree) and (6) distance to rivers (m) with a catchment area $> 10^5 \text{ m}^2$ (ref. ⁷⁴). We also use (7) distance to built-up land⁶⁷ (m) and (8) distance to roads (m) (retrieved in OpenStreetMap⁸) as deforestation predictors. All spatial layers were resampled to the resolution of the regional forest-cover data, that is, 30 m.

The layout of built-up land and roads has changed over time; hence we investigate the compatibility of the 1958 and 2016 data. If there is no agreement, we cannot use these data to construct predictive variables for past deforestation. First, we identify all urban clusters in 2016, defined as an isolated and contiguous area consisting solely of built-up land. Second, we randomly sample 1,000 cluster instances and assess whether each of these built-up areas was already present in 1958. The historical compatibility of the road data is assessed through calculating the proportion of roads (kilometre road in 1958 per kilometre road in 2016) that

were already present in 1958. When reconstructing historical deforestation prior to 2001, we exclude the roads that were not present in 1958 as a predictor variable.

For the validation of the deforestation likelihood model, we assess the area under the curve (AUC) of the receiver operating characteristic (ROC). The AUC ranges between 0 and 1 and is a measure for the discriminatory power of the model⁷⁵. To obtain a robust estimate of the AUC, we apply 10-fold cross-validation^{29,76}; the deforestation and conservation data are split randomly into 10 subsets. Subsequently, we use nine parts to train a model that is validated with the remaining tenth part of the data. This procedure is iterated 10 times, each time using a different data subset for model validation. The average of these 10 AUC estimates is considered a robust model-performance statistic⁷⁶.

We investigate the importance of the different deforestation predictors by means of McFadden's pseudo R^2 (ρ^2). This statistic is a measure for the variance explained by the model and values between 0.2 and 0.4 generally indicate an excellent model fit^{77,78}. We assess the importance of each variable by training and validating models using only the considered variable. We can use the ρ^2 of such a model to estimate the proportion of variance explained by each predictor. We repeat this investigation for the three different time periods (1958–1988, 1988–2001 and 2001–2016). For the periods 1958–1988 and 1988–2001 we cannot investigate the importance of deforestation contagion as we do not have annual data available to train these two deforestation models.

The annual deforestation rate N_{def} is assumed to be dynamic in time (Supplementary Methods). It is calculated based on the assumption that the initial deforestation rate in all 3 countries doubles every 20 years in the period 1958–1988, considering more general deforestation trends in the central African rainforest⁷⁹ and the fact that the populations in Rwanda, Burundi and the DRC have grown at a similar rate⁷. Between 1988 and 2001, the estimation of N_{def} in the DRC and Rwanda is complicated by political conflicts that induced refugee fluxes and internal displacement, causing an accelerated forest decline^{37,38}. Therefore, we assume for these countries a tripling of the deforestation rate in 1994. Between 2001 and 2016, we derive the deforestation rates in all three countries from the global forest data⁷¹.

Similarly to the deforestation pattern, we reconstruct the afforestation pattern by means of a logistic regression model predicting the annual afforestation likelihood. The outcome of this model is again a binary variable (afforested/not afforested). Here, we select the same independent variables as for the deforestation likelihood model, with the exception of the deforestation contagion factor. In total, 7,000 training samples are generated randomly from the global forest-cover-change data⁷¹ (these global data were also validated with the regional and continental forest data^{66,67}). An equal-shares sampling design for the afforested/not afforested data is applied. For every year between 1958 and 2016, we recalculate the afforestation likelihood and convert the N_{aff} non-forest pixels with the highest predicted value into forest pixels. The number N_{aff} is derived as the total number of afforested pixels between two given images divided by the number of years covered by those images. Hence, we assume the annual afforestation rate to be invariable in time. We assess the model quality and variable importance by means of the 10-fold cross-validation and the analysis of the univariate ρ^2 .

Landslide hazard and forest-cover changes. To link the annual forest-cover pattern to the shallow landslide hazard, we apply a two-step modelling approach proposed by Broeckx et al.⁸⁰ where we first calculate the annual shallow landslide susceptibility (LSS) and subsequently link the LSS to the shallow landslide hazard. The landslide hazard is defined as the probability of landslide occurrence (and associated magnitude) within a certain time frame and area¹⁴. Hence, within this study, we calculate landslide hazard as the total affected area per km^2 per year ($\text{m}^2 \text{ km}^{-2} \text{ yr}^{-1}$).

For the calibration of both the LSS and hazard model, we rely on (1) the shallow landslide inventory presented by Depicker et al.²⁰ and Depicker et al.²⁹ that was compiled by visually assessing 932 Google Earth images from 2000 to 2019, and (2) the global forest-cover-change data for the period 2000–2017⁷¹. Both the landslide and forest data are corrected with the regional and continental forest-cover data^{66,67} (the 'Annual forest-cover changes' section). As such, we retain 4,367 validated landslide instances that are used to calibrate our models. The total affected area of these landslides ranges from ~ 10 to $\sim 10,000 \text{ m}^2$ and is on average 781 m^2 . Within this inventory, we observe three common landslide types, or a combination thereof: debris slides, avalanches and debris/mud flows⁸¹.

Landslide susceptibility assessment. We develop a LSS model to predict the absence/presence of landslides based on logistic regression (equation (1)). Moreover, this LSS model responds to deforestation and afforestation so that we can examine the evolution of the shallow LSS by linking it to the (reconstructed) annual changes in forest cover (the 'Annual forest-cover changes' section). However, the effect of forest cover and deforestation in this region is shown to be dependent on landscape rejuvenation²⁰. Active rifting and the associated tectonic uplift induce the upstream migration of knickpoints, that is, a sudden and steep increase in the river profile (often a waterfall) that forms the boundary between a 'younger' downstream rejuvenated landscape and an 'older' upstream relict landscape. These two types of landscape within the Kivu Rift display a different response to forest coverage and deforestation as a result of differences in seismicity, regolith thickness

and climate²⁰. We therefore include a land-cover variable in our LSS model that integrates the interaction between land cover and landscape rejuvenation. In total, we distinguish five land-cover classes: (1) forest inside the rejuvenated areas, (2) forest in relict areas, (3) non-forest in rejuvenated areas, (4) non-forest in relict areas and (5) areas deforested less than 15 years ago (the duration of the deforestation-induced landslide wave)²⁰.

In 7.2% of the study area, the situation arises that non-forest land is afforested and afterwards deforested again. We do not know whether the landslide response of 'new' forests is the same as for primary forest. Hence, we run the hazard simulations twice, one time assuming that cutting new forests causes a landslide wave similar to that caused by the cutting of primary forest, and a second time assuming that the removal of new forests does not cause a deforestation-induced landslide wave. The landslide literature favours the latter scenario^{10,20}. Generally, a new landslide equilibrium will be established within ~15 years after deforestation²⁰. This implies that if forest is allowed to re-establish >15 years after initial deforestation and is consequently removed, the landscape simply returns to the equilibrium situation reached after the first deforestation event and no extra landslides are to be expected.

Beside the categorical land-cover variable, we use six additional predictor variables within our LSS analysis, as a previous study in the region has confirmed that these variables are of intermediate to high importance for predicting LSS²⁹: slope, planar curvature, profile curvature, distance to drainage and the east exposure. Lastly, we include imagery density, that is, number of available images in Google Earth for a certain location, as it may affect the total number of instances observed in our shallow landslide inventory²⁰. By taking into account imagery density, we avoid a bias in the LSS calculations, as a higher imagery density will allow for better landslide detection and thus a higher LSS²⁰. The imagery density data are retrieved from Depicker et al.²⁰. To remediate the imagery density bias, we first calibrate the LSS model with the original (biased) imagery density data and subsequently reconstruct the annual LSS from 1958 to 2016 by assuming an equal, fixed density of five images (the average imagery density) for the entire study area. The spatial pattern of extreme rainfall (which is the main trigger for the observed landslides) is not included in the susceptibility analysis, as previous LSS assessments in the region showed a very weak effect²⁹.

For the calibration and validation of the LSS model we use our 4,367 landslide observation points in combination with 11,580 randomly sampled non-landslide points. The number of non-landslide points is large enough to ensure a proper representation of the different land-cover classes. We assess the model quality by means of the 10-fold cross-validation. We use the susceptibility model to make a first estimation of the impact of deforestation and afforestation on landslide occurrence by calculating the odds ratios for the different dummy variables that represent the forest cover.²⁹

Hazard as a function of susceptibility. We link the LSS to the landslide hazard by assessing the average hazard in different subregions that are delineated according to their susceptibility. The first subregion encompasses all areas with an LSS value between 0 and 0.1, the second subregion all areas with an LSS value between 0.1 and 0.2, and so on. For each subregion and its associated landslides, we apply the following equation, proposed by Depicker et al.²⁰:

$$\text{hazard}_i = \frac{1}{A_i} \sum_{j=1}^{n_i} \frac{a_{\text{tot}}^j}{r^j}, \quad (2)$$

whereby hazard_i is the average landslide hazard in the i th of our 10 subregions, A_i the total surface area (km²) of subregion i , a_{tot}^j the total affected area (m²) of the j th of n_i observed landslides (with n_i the number of landslides in subregion i) and r^j the Google Earth imagery range (years) observed in landslide j . The imagery range data are retrieved from the work of Depicker et al.²⁰ whereby the range is defined as the age difference between the oldest and newest image available at the landslide location. Finally, we couple these 10 hazard observations to the 10 median LSS values of the subregions by means of an adjusted logistic regression (Fig. 4a), which we found to yield a better fit than linear models:

$$\text{hazard} = \frac{H_{\text{max}}}{1 + e^{-(\alpha_0 + \beta_1 \text{LSS})}}, \quad (3)$$

where H_{max} is the maximum of the 10 observed hazard values in the subregions, α_0 is the intercept and β_1 is the coefficient for variable LSS.

Using equation (3), we convert the annual LSS (with continuous values between 0 and 1) into an annual landslide hazard map (continuous values between 0 and H_{max}). To estimate the proportion of hazard that is attributed to deforestation, we compare the current results with a benchmark scenario in which no deforestation has taken place since 1958.

Uncertainty of hazard and susceptibility. The susceptibility model and susceptibility-hazard relationship are only calibrated for contemporary data between 2001 and 2016. Nevertheless, we assume these models are applicable to historical landscapes prior to the year 2000. This assumption is supported by the notion that the conditions governing susceptibility, with the exception of

forest cover, have remained stable within our observation period (slope, aspect, curvature and distance to rivers). Furthermore, we cannot fully characterize the deforestation-induced landslide wave (lasting approximately 15 years²⁰) between 1958 and 1973, given that no forest data prior to 1958 are available.

For the susceptibility and hazard calculations, we assume that the historical changes are driven by deforestation and afforestation and that they are not influenced by other environmental changes such as changes in rainfall patterns. This approach is justified as human disturbances (such as forest-cover changes), when compared with climatic variations, are expected to have a larger impact on changes in landslide hazard at the decadal timescale^{12,41}. Moreover, contrary to the widespread forest-cover changes in the region, evidence for any decadal trends in extreme rainfall events (positive or negative) is weak.^{42,43}

The uncertainty of the final landslide hazard estimates will depend, to a large extent, on the uncertainty associated with the LSS model that is used to translate forest cover into landslide hazard. We apply Efron's bootstrap⁸² to budget the landslide hazard uncertainty arising from the LSS model: the LSS and hazard calculations are iterated 200 times, each time recalibrating the LSS model (as well as the hazard = $f(\text{LSS})$ relationship) with a training dataset that is a random sample (with replacement) from the original training dataset and has an equal size. These 200 results are expected to fall between the lower and upper limits of the 80% confidence interval.⁸²

Risk based on hazard and exposure. We define landslide risk as the expected number of fatalities, calculated as the combination of the hazard (where and how often do landslides occur?), the exposure (who could encounter a landslide?) and the vulnerability of the people (the mortality probability when a person encounters a landslide)¹⁵. However, no quantitative information on vulnerability is available for the Kivu Rift. Moreover, a vulnerability assessment is hampered by data and fieldwork constraints. We assume that the vulnerability in the Kivu Rift is high due to poor housing quality, the absence of early warning systems and a lack of mobility during nighttime and/or heavy rain (the dominant landslide trigger in the study area⁶⁰). Moreover, we consistently underestimate the hazard (and thus the risk), as hazard is directly derived from a landslide inventory that could potentially be incomplete (the 'Landslide hazard and forest-cover changes' section). The potential incompleteness stems from biases in the available Google Earth imagery used to detect those landslides²⁰ and/or the difficulty of visually assessing landslides that have a small total affected area.

Assuming that there are no large regional differences in vulnerability and considering that our objective is to compare the relative risk between regions rather than obtaining accurate estimates of the expected number of fatalities, we adopt a fixed vulnerability factor of 1. Hence, we approximate risk as the product of hazard and exposure. Moreover, risk is expressed as the expected number of people affected per 100,000 inhabitants per year (the incidence). It is calculated by multiplying the landslide hazard (the 'Landslide hazard and forest-cover changes' section) with population density^{4,31} and subsequently dividing this number by the entire population.

The population density is assessed through the spatially explicit Global Human Settlement Layer⁴⁶, which is provided for four years: 1975, 1990, 2000 and 2015. The data are available at: <http://ghsl.jrc.ec.europa.eu/>. The gridded data are the result of detecting the built-up land in satellite imagery and subsequently calculating the average population density per built-up pixel (at a 30 m resolution) by means of regional/national census data. Although these data overall give a realistic image of the population density at different times, they have some visible artefacts, especially in the 1975 data, such as large surfaces (typically administrative regions) with homogeneous population density.

To assess the contribution of deforestation to risk in a certain year, we compare the estimated risk with a scenario with no forest-cover changes since 1958. More precisely, this benchmark risk is calculated by multiplying the population density in that year with the hazard calculated for 1958.

Reporting Summary. Further information on research design is available in the Nature Research Reporting Summary linked to this article.

Data availability

The 1958 forest-cover data can be accessed at: <https://doi.org/10.5281/zenodo.5027117>. The 1958 panchromatic orthomosaics will be available at the end of the PASTECA project in March 2022 (<http://pasteca.africamuseum.be/data>). The landslide inventory is provided by Depicker et al.²⁰ (<https://doi.org/10.5194/esurf-9-445-2021>) and can be downloaded at: <https://doi.org/10.5281/zenodo.5027004>. The land-cover data for 1988 and 2001 are provided by Basnet and Vodacek⁶⁶ (<https://doi.org/10.3390/rs70606683>). The 2016 land-cover data are provided by ESA and can be accessed at: <http://2016africalandcover20m.esrin.esa.int/>. The population-density data are derived from the Global Human Settlement Layer that can be accessed at: <http://ghsl.jrc.ec.europa.eu/>. The Shuttle Radar Topography Mission digital elevation model is provided by the US Geological Survey (<https://earthexplorer.usgs.gov/>). The seismic data (Peak Ground Acceleration) are provided by Delvaux et al.⁸³ (<https://doi.org/10.1016/j.jafrearsci.2016.10.004>) upon contacting the corresponding author. The road data can be downloaded from OpenStreetMap (<https://www.openstreetmap>).

org/#map=7/50.510/4.475). The Global Forest Change 2000–2019 data from Hansen et al.⁷¹ can be found at: <https://data.globalforestwatch.org/documents/14228e6347c44f5691572169e9e107ad/explore>. The lithology data are retrieved from the work of Depicker et al.²⁹ (<https://doi.org/10.1016/j.geomorph.2019.106886>) and can be requested from the author. The raw data used for Figs. 3–5 in this work can be accessed at: <https://doi.org/10.6084/m9.figshare.14838825>. Source data are provided with this paper.

Code availability

The Python code used to derive the forest cover from aerial photographs and reconstruct the forest-cover changes can be requested from the corresponding authors.

Received: 22 January 2021; Accepted: 9 July 2021;

Published online: 19 August 2021

References

- McBean, G. A. Integrating disaster risk reduction towards sustainable development. *Curr. Opin. Environ. Sustain.* **4**, 122–127 (2012).
- Kelman, I. Linking disaster risk reduction, climate change, and the sustainable development goals. *Disaster Prev. Manag.* **26**, 254–258 (2017).
- United Nations Department of Economic and Social Affairs *World Population Prospects 2019* (United Nations, accessed 16 July 2020); population.un.org/wpp/
- Ehrlich, D. et al. Remote sensing derived built-up area and population density to quantify global exposure to five natural hazards over time. *Remote Sens.* **10**, 1378 (2018).
- Lambin, E. F. & Meyfroidt, P. Global land use change, economic globalization, and the looming land scarcity. *Proc. Natl Acad. Sci. USA* **108**, 3465–3472 (2011).
- Chamberlin, J., Jayne, T. S. & Headey, D. Scarcity amidst abundance? Reassessing the potential for cropland expansion in Africa. *Food Policy* **48**, 51–65 (2014).
- Nkonya, E., Mirzabaev, A. & von Braun, J. (eds) *Economics of Land Degradation and Improvement—A Global Assessment for Sustainable Development* (Springer, 2015).
- Young, A. Poverty, hunger and population policy: linking Cairo with Johannesburg. *Geogr. J.* **171**, 83–95 (2005).
- Mugagga, F., Kakembo, V. & Buyinza, M. Land use changes on the slopes of Mount Elgon and the implications for the occurrence of landslides. *Catena* **90**, 39–46 (2012).
- Sidle, R. C. & Bogaard, T. A. Dynamic Earth system and ecological controls of rainfall-initiated landslides. *Earth Sci. Rev.* **159**, 275–291 (2016).
- Kirschbaum, D., Stanley, T. & Zhou, Y. Spatial and temporal analysis of a global landslide catalog. *Geomorphology* **249**, 4–15 (2015).
- Froude, M. J. & Petley, D. N. Global fatal landslide occurrence from 2004 to 2016. *Nat. Hazard Earth Syst. Sci.* **18**, 2161–2181 (2018).
- Reichenbach, P., Rossi, M., Malamud, B. D., Mihir, M. & Guzzetti, F. A review of statistically-based landslide susceptibility models. *Earth Sci. Rev.* **180**, 60–91 (2018).
- Guzzetti, F., Reichenbach, P., Cardinali, M. & Ardizzone, A. Probabilistic landslide hazard assessment at the basin scale. *Geomorphology* **72**, 272–299 (2005).
- Corominas, C. et al. Recommendations for the quantitative analysis of landslide risk. *Bull. Eng. Geol. Environ.* **73**, 209–263 (2014).
- Ray, R. L., Jacobs, J. M. & Ballesterio, T. P. Regional landslide susceptibility: spatiotemporal variations under dynamic soil moisture conditions. *Nat. Hazards* **59**, 1317–1337 (2011).
- Reichenbach, P., Busca, C., Mondini, A. C. & Rossi, M. The influence of land use change on landslide susceptibility zonation: the Briga Catchment test site (Messina, Italy). *Environ. Manag.* **54**, 1372–1384 (2014).
- Hua, Y., Wang, X., Li, Y., Xu, P. & Xia, W. Dynamic development of landslide susceptibility based on slope unit and deep neural networks. *Landslides* **18**, 281–302 (2021).
- Montgomery, D., Schmidt, K., Greenberg, H. & Dietrich, W. Forest clearing and regional landsliding. *Geology* **28**, 311–314 (2000).
- Depicker, A. et al. Interactions between deforestation, landscape rejuvenation, and shallow landslides in the North Tanganyika–Kivu Rift region, Africa. *Earth Surf. Dyn.* **9**, 445–462 (2021).
- Knapen, A. et al. Landslides in a densely populated country at the footslopes of Mount Elgon (Uganda): characteristics and causal factors. *Geomorphology* **73**, 149–165 (2006).
- Kucsicsa, G. et al. Assessing the potential future forest-cover change in Romania, predicted using a scenario-based modelling. *Environ. Model. Assess.* **25**, 471–491 (2020).
- Dolidon, N., Hofer, T., Jansky, L. & Sidle, R. in *Landslides: Disaster Risk Reduction* (eds Sasa, K. & Canuti, P.) 633–649 (Springer, 2009).
- Moos, C. et al. Ecosystem-based disaster risk reduction in mountains. *Earth Sci. Rev.* **177**, 497–513 (2018).
- de Jesús Arce-Mojica, T., Nehren, U., Sudmeier-Rieux, K., Miranda, P. J. & Anhof, D. Nature-based solutions (NbS) for reducing the risk of shallow landslides: where do we stand? *Int. J. Disaster Risk Reduct.* **41**, 101293 (2019).
- Maes, J. et al. Landslide risk reduction measures: a review of practices and challenges for the tropics. *Prog. Phys. Geogr.* **41**, 191–221 (2017).
- Monsieurs, E. et al. Landslide inventory for hazard assessment in a data-poor context: a regional-scale approach in a tropical African environment. *Landslides* **15**, 2195–2209 (2018).
- Delvaux, D. & Barth, A. African stress pattern from formal inversion of focal mechanism data. *Tectonophysics* **482**, 105–128 (2010).
- Depicker, A. et al. The added value of a regional landslide susceptibility assessment: the western branch of the East African Rift. *Geomorphology* **353**, 106886 (2020).
- Dewitte, O. et al. Constraining landslide timing in a data-scarce context: from recent to very old processes in the tropical environment of the North Tanganyika–Kivu Rift region. *Landslides* **18**, 161–177 (2021).
- Emberson, R., Kirschbaum, D. & Stanley, T. New global characterisation of landslide exposure. *Nat. Hazards Earth Syst. Sci.* **20**, 3413–3424 (2020).
- National Contingency Plan for Floods and Landslides* (Ministry in Charge of Emergency Management of the Republic of Rwanda, 2018); https://www.minema.gov.rw/fileadmin/user_upload/Minema/Publications/Contingency_Plans/Contingency_Plan_for_Floods_nd_Landslides.pdf
- Aleman, J. C., Jarzyna, M. A. & Staver, A. C. Forest extent and deforestation in tropical Africa since 1900. *Nat. Ecol. Evol.* **2**, 26–33 (2018).
- Ellis, E. C., Goldewijk, K. K., Siebert, S., Lightman, D. & Ramankutty, N. Anthropogenic transformation of the biomes, 1700 to 2000. *Glob. Ecol. Biogeogr.* **19**, 589–606 (2010).
- Stebbing, E. P. Forests of the Belgian Congo. *Nature* **172**, 1177 (1953).
- Kleinschroth, F., Laporte, N., Laurance, W. F., Goetz, S. J. & Ghazoul, J. Road expansion and persistence in forests of the Congo Basin. *Nat. Sustain.* **2**, 628–634 (2019).
- Gachuruzi, S. B. The impact of refugees on the environment: the case of Rwandan refugees in Kivu, Zaire. *Refuge* **15**, 24–26 (1996).
- Huggins, C. & Clover, J. (eds) *From the Ground Up: Land Rights, Conflict and Peace in Sub-Saharan Africa* (ISS, 2005).
- Garrett, N., Sergiou, S. & Vlassenroot, K. Negotiated peace for extortion: the case of Walikale territory in eastern DR Congo. *J. East. Afr. Stud.* **3**, 1–21 (2009).
- Butsic, V., Baumann, M., Shortland, A., Walker, S. & Kuemmerle, T. Conservation and conflict in the Democratic Republic of Congo: the impacts of warfare, mining, and protected areas on deforestation. *Biol. Conserv.* **191**, 266–273 (2015).
- Muñoz-Torrero Manchado, A. et al. Three decades of landslide activity in western Nepal: new insights into trends and climate drivers. *Landslides* **18**, 2001–2015 (2021).
- Chaney, N. W., Sheffield, J., Villarini, G. & Wood, E. F. Development of a high-resolution gridded daily meteorological dataset over sub-Saharan Africa: spatial analysis of trends in climate extremes. *J. Clim.* **27**, 5815–5835 (2014).
- Omondi, P. A. O. et al. Changes in temperature and precipitation extremes over the Greater Horn of Africa Region from 1961 to 2010. *Int. J. Climatol.* **34**, 1262–1277 (2014).
- Leurquin, P. P. Agricultural change in Ruanda–Urundi: 1945–1960. *Food Res. Inst. Stud.* **4**, 1–51 (1963).
- Meditz, S. W., Merrill, T. & Library of Congress, Federal Research Division (eds) *Zaire: A Country Study* 4th edn (Library of Congress, 1994).
- GHS Population Grid, Derived from GPW4, Multitemporal (1975, 1990, 2000, 2015)* (European Commission, JRC, accessed 12 August 2020); http://data.europa.eu/89h/jrc-ghsl-ghs_pop_gpw4_globe_r2015a
- Kanyambwa, S. Impact of war on conservation: Rwandan environment and wildlife in agony. *Biodivers. Conserv.* **7**, 1399–1406 (1998).
- Ordway, E. M. Political shifts and changing forests: effects of armed conflict on forest conservation in Rwanda. *Glob. Ecol. Conserv.* **3**, 448–460 (2015).
- Michellier, C., Pigeon, P., Kervyn, F. & Wolff, E. Contextualizing vulnerability assessment: a support to geo-risk management in central Africa. *Nat. Hazards* **82**, S27–S42 (2016).
- Banerjee, O. et al. Economic, land use, and ecosystem services impacts of Rwanda's Green Growth Strategy: an application of the IEEM + ESM platform. *Sci. Total Environ.* **729**, 138779 (2020).
- Vervisch, T., Titeca, K., Vlassenroot, K. & Braeckman, J. Social capital and post-conflict reconstruction in Burundi: the limits of community-based reconstruction. *Dev. Change* **44**, 147–174 (2013).
- Reyntjens, F. *The Great African War—Congo and Regional Geopolitics, 1996–2006* (Cambridge Univ. Press, 2009).
- De Putter, T. & Delvaux, C. Certifier les ressources minérales dans la région des Grands Lacs. *Polit. Etrang.* **2**, 99–112 (2013).
- Nassar, N. T. Shifts and trends in the global anthropogenic stocks and flows of tantalum. *Resour. Conserv. Recycl.* **125**, 233–250 (2017).
- Maps of Conflict Minerals in Eastern DRC—A0 Posters* (International Peace Information Service, accessed 25 September 2020); <https://ipisresearch.be/publication/map-conflict-minerals-eastern-drc-a0-posters/>

56. van Acker, F. Where did all the land go? Enclosure & social struggle in Kivu (D.R. Congo). *Rev. Afr. Polit. Econ.* **32**, 79–98 (2005).
57. Luethje, E., Kranz, O. & Schoepfer, E. Geographic object-based image analysis using optical satellite imagery and GIS data for the detection of mining sites in the Democratic Republic of the Congo. *Remote Sens.* **6**, 6636–6661 (2014).
58. Tyukavina, A. et al. Congo Basin forest loss dominated by increasing smallholder clearing. *Sci. Adv.* **4**, eaat2993 (2018).
59. Günter, S., Weber, M., Erreis, R. & Aguirre, N. Influence of distance to forest edges on natural regeneration of abandoned pastures: a case study in the tropical mountain rain forest of southern Ecuador. *Eur. J. For. Res.* **126**, 67–75 (2007).
60. Pollock, W. & Wartman, J. Human vulnerability to landslides. *GeoHealth* **4**, e2020GH000287 (2020).
61. Vlassenroot, K. & Raeymaekers, T. *Conflict and Social Transformation in Eastern DR Congo* (Academia Press, 2005).
62. Lehmann, P., Von Ruetze, J. & Or, D. Deforestation effects on rainfall-induced shallow landslides: remote sensing and physically-based modelling. *Water* **55**, 9962–9976 (2019).
63. Meyfroidt, P. & Lambin, E. F. Global forest transition: prospects for an end to deforestation. *Annu. Rev. Environ. Resour.* **36**, 343–371 (2011).
64. Willemen, L. et al. How to halt the global decline of lands. *Nat. Sustain.* **3**, 164–166 (2020).
65. Corbane, C. et al. A global cloud free pixel-based image composite from Sentinel-2 data. *Data Brief* **31**, 105737 (2020).
66. Basnet, B. & Vodacek, A. Tracking land use/land cover dynamics in cloud prone areas using moderate resolution satellite data: a case study in Central Africa. *Remote Sens.* **7**, 6683–6709 (2015).
67. *ESA Climate Change Initiative–Land Cover Project 2017. 20 m Resolution* (European Space Agency, 2016).
68. He, F., Li, S. & Zhang, X. A spatially explicit reconstruction of forest cover in China over 1700–2000. *Glob. Planet. Change* **131**, 73–81 (2015).
69. Bolliger, J., Schmatz, D., Pazúr, R., Ostapowicz, K. & Psomas, A. Reconstructing forest-cover change in the Swiss Alps between 1880 and 2010 using ensemble modelling. *Reg. Environ. Change* **17**, 2265–2277 (2017).
70. Hosmer, D. W. & Lemeshow, S. *Applied Logistic Regression* 2nd edn (John Wiley & Sons, 2000).
71. Hansen, M. C. et al. High-resolution global maps of 21st-century forest cover change. *Science* **342**, 850–853 (2013).
72. Rosa, I. M., Purves, D., Souza, C. & Ewers, R. M. Predictive modelling of contagious deforestation in the Brazilian Amazon. *PLoS ONE* **8**, e77231 (2013).
73. Poor, E. E., Jati, V. I., Imron, M. A. & Kelly, M. J. The road to deforestation: edge effects in an endemic ecosystem in Sumatra, Indonesia. *PLoS ONE* **14**, e0217540 (2019).
74. USGS Shuttle Radar Topography Mission, *Global Land Cover Facility. 1 Arc-Second* (Univ. of Maryland, 2006).
75. Fawcett, T. An introduction to ROC analysis. *Pattern Recognit. Lett.* **27**, 861–874 (2006).
76. Brenning, A. Improved spatial analysis and prediction of landslide susceptibility: practical recommendations. In *Landslides and Engineered Slopes: Protecting Society Through Improved Understanding. Proc. 11th International and 2nd North American Symposium on Landslides and Engineered Slopes* (eds Eberhardt, E. et al.) 789–794 (CRC Press/Balkema, 2012).
77. McFadden, D. in *Frontiers in Econometrics* (ed. Zarembka, P.) 105–142 (Academic Press, 1973).
78. McFadden, D. in *Behavioural Travel Modelling* (eds Hensher, D. & Stopher, P.) 279–318 (Croom Helm, 1978).
79. Rosa, I. M., Smith, M. J., Wearn, O. R., Purves, D. & Ewers, R. M. The environmental legacy of modern tropical deforestation. *Curr. Biol.* **26**, 2161–2166 (2016).
80. Broeckx, J. et al. Landslide susceptibility and mobilization rates in the Mount Elgon region, Uganda. *Landslides* **16**, 571–584 (2019).
81. Hungr, O., Lerouel, S. & Picarelli, L. The Varnes classification of landslide types, an update. *Landslides* **11**, 167–194 (2014).
82. Harrell, F. E. *Regression Modeling Strategies: With Applications to Linear Models, Logistic and Ordinal Regression, and Survival Analysis* 2nd edn (Springer, 2003).
83. Delvaux, D. et al. Seismic hazard assessment of the Kivu Rift segment based on a new seismotectonic zonation model (western branch, East African Rift system). *J. Afr. Earth Sci.* **134**, 831–855 (2017).

Acknowledgements

This study was supported by the Belgium Science Policy Office (BELSPO) through the PASTeCA project (BR/165/A3/PASTeCA) entitled 'Historical Aerial Photographs and Archives to Assess Environmental Changes in Central Africa' (<http://pasteca.africamuseum.be/>). We further wish to thank F. Canters, F. Makanzu Imwangana, A. M. C. Umutoni, G. Sakindi, J. van Vliet and T. De Putter for their insightful discussions and recommendations regarding this research.

Author contributions

A.D., L.J., G.G. and O.D. designed the study. A.D. developed the models and carried out the analyses. A.D. wrote the paper and designed the figures, with input from L.J., G.G. and O.D. B.S. and F.K. organized and processed the historical aerial photographs. B.S. and A.D. created the panchromatic orthomosaic. N.M., M.L. and E.W. developed the algorithms to classify the orthomosaic into forest. C.M. contributed to the historical analysis of the societal drivers. A.V.R. contributed to the design of the land-cover methodology. All authors proofread and commented on the manuscript.

Competing interests

The authors declare no competing interests.

Additional information

Supplementary information The online version contains supplementary material available at <https://doi.org/10.1038/s41893-021-00757-9>.

Correspondence and requests for materials should be addressed to A.D. or O.D.

Peer review information *Nature Sustainability* thanks Fritz Kleinschroth, Faith E. Taylor and Anthony Vodacek for their contribution to the peer review of this work.

Reprints and permissions information is available at www.nature.com/reprints.

Publisher's note Springer Nature remains neutral with regard to jurisdictional claims in published maps and institutional affiliations.

© The Author(s), under exclusive licence to Springer Nature Limited 2021

Reporting Summary

Nature Portfolio wishes to improve the reproducibility of the work that we publish. This form provides structure for consistency and transparency in reporting. For further information on Nature Portfolio policies, see our [Editorial Policies](#) and the [Editorial Policy Checklist](#).

Statistics

For all statistical analyses, confirm that the following items are present in the figure legend, table legend, main text, or Methods section.

n/a Confirmed

- The exact sample size (n) for each experimental group/condition, given as a discrete number and unit of measurement
- A statement on whether measurements were taken from distinct samples or whether the same sample was measured repeatedly
- The statistical test(s) used AND whether they are one- or two-sided
Only common tests should be described solely by name; describe more complex techniques in the Methods section.
- A description of all covariates tested
- A description of any assumptions or corrections, such as tests of normality and adjustment for multiple comparisons
- A full description of the statistical parameters including central tendency (e.g. means) or other basic estimates (e.g. regression coefficient) AND variation (e.g. standard deviation) or associated estimates of uncertainty (e.g. confidence intervals)
- For null hypothesis testing, the test statistic (e.g. F , t , r) with confidence intervals, effect sizes, degrees of freedom and P value noted
Give P values as exact values whenever suitable.
- For Bayesian analysis, information on the choice of priors and Markov chain Monte Carlo settings
- For hierarchical and complex designs, identification of the appropriate level for tests and full reporting of outcomes
- Estimates of effect sizes (e.g. Cohen's d , Pearson's r), indicating how they were calculated

Our web collection on [statistics for biologists](#) contains articles on many of the points above.

Software and code

Policy information about [availability of computer code](#)

Data collection

The landslide inventory and the Google Earth imagery density and range data were retrieved from the work of Depicker et al. 2021 (<https://doi.org/10.5194/esurf-9-445-2021>) and can be accessed at <https://doi.org/10.5281/zenodo.5027004>. The historical photographs are conserved at the Royal Museum for Central Africa in Belgium (<http://pasteca.africamuseum.be/home>). Other used datasets include:

- the land cover data for 1988 and 2001, provided by Basnet and Vodacek, 2015 (<https://doi.org/10.3390/rs70606683>)
- the 2016 land cover data, provided by ESA (<http://2016africalandcover20m.esrin.esa.int/>)
- the Global Human Settlement Layer (GHSL), be accessed at <http://ghsl.jrc.ec.europa.eu/>
- the SRTM digital elevation model, provided by the USGS (<https://earthexplorer.usgs.gov/>)
- the seismic data (PGA), provided by Delvaux et al. (2017) (<http://dx.doi.org/10.1016/j.jafrearsci.2016.10.004>)
- the road data, downloaded from OpenStreetMap (<https://www.openstreetmap.org/#map=7/50.510/4.475>)
- the Global Forest Change 2000-2019, found at <https://data.globalforestwatch.org/documents/14228e6347c44f5691572169e9e107ad/explore>
- the lithology data, retrieved from the work of Depicker et al. (2020) (<https://doi.org/10.1016/j.geomorph.2019.106886>) and can be requested from the author.

Data analysis

We used the following software for our analysis:

- Python v3.5 (<https://www.anaconda.com/products/individual>)
- QGIS 3 (<https://www.qgis.org/nl/site/forusers/download.html>)
- Agisoft Metashape Pro (<https://www.agisoft.com/>)
- Cloud Compare (<https://www.danielgm.net/cc/>)

We used the Python code from Mboga et al. (2020) (<https://doi.org/10.1016/j.isprsjprs.2020.07.005>) to classify the panchromatic orthomosaic into forest cover classes. For all other analyses, we developed custom Python scripts which can be requested from the corresponding authors.

For manuscripts utilizing custom algorithms or software that are central to the research but not yet described in published literature, software must be made available to editors and reviewers. We strongly encourage code deposition in a community repository (e.g. GitHub). See the Nature Portfolio [guidelines for submitting code & software](#) for further information.

Data

Policy information about [availability of data](#)

All manuscripts must include a [data availability statement](#). This statement should provide the following information, where applicable:

- Accession codes, unique identifiers, or web links for publicly available datasets
- A description of any restrictions on data availability
- For clinical datasets or third party data, please ensure that the statement adheres to our [policy](#)

The 1958 forest cover data can be accessed at <https://doi.org/10.5281/zenodo.5027117>. The 1958 panchromatic orthomosaics will become available at the end of the PASTeCA project in March 2022 (<http://pasteca.africamuseum.be/data>). The landslide inventory is provided by Depicker et al. (2021) (<https://doi.org/10.5194/esurf-9-445-2021>) and can be downloaded at <https://doi.org/10.5281/zenodo.5027004>. The land cover data for 1988 and 2001 are provided by Basnet and Vodacek (2015) (<https://doi.org/10.3390/rs70606683>). The 2016 land cover data are provided by ESA and can be accessed at <http://2016africalandcover20m.esrin.esa.int/>. The population density data were derived from the Global Human Settlement Layer (GHSL) which can be accessed at <http://ghsl.jrc.ec.europa.eu/>. The SRTM digital elevation model was provided by the USGS (<https://earthexplorer.usgs.gov/>). The seismic data (PGA) were provided by Delvaux et al. (2017) (<http://dx.doi.org/10.1016/j.jafrearsci.2016.10.004>) upon contacting the corresponding author. The road data were downloaded from OpenStreetMap (<https://www.openstreetmap.org/#map=7/50.510/4.475>). The Global Forest Change 2000-2019 data from Hansen et al. (2013) can be found at <https://data.globalforestwatch.org/documents/14228e6347c44f5691572169e9e107ad/explore>. The lithology data was retrieved from the work of Depicker et al. (2020) (<https://doi.org/10.1016/j.geomorph.2019.106886>) and can be requested from the author. The raw data used for Fig. 3, Fig. 4, and Fig. 5 in this work can be accessed at <https://doi.org/10.6084/m9.figshare.14838825>.

Field-specific reporting

Please select the one below that is the best fit for your research. If you are not sure, read the appropriate sections before making your selection.

- Life sciences Behavioural & social sciences Ecological, evolutionary & environmental sciences

For a reference copy of the document with all sections, see nature.com/documents/nr-reporting-summary-flat.pdf

Ecological, evolutionary & environmental sciences study design

All studies must disclose on these points even when the disclosure is negative.

Study description

We use historical panchromatic aerial photographs and regional land cover maps to reconstruct the annual forest dynamics in the Kivu Rift and we apply these data to model the multi-decadal dynamics of landslide susceptibility, hazard, and risk. We use nearly 2,400 photographs from 1958 to construct an orthomosaic that reveals the forest cover in the study area. We combine this historical forest map with more recent regional land cover products to recreate the annual forest cover changes between 1958 and 2016. Subsequently, we use an existing landslide inventory to (i) develop a dynamic landslide susceptibility model that responds to forest cover changes and (ii) calibrate the relationship between susceptibility and hazard. As such, the annual forest data allow to assess the evolution of the landslide hazard. Finally, the annual landslide hazard is combined with the distribution of the population density at different points in time to quantify historical trends in landslide risk.

Research sample

We used 4,376 landslides to calculate the landslide susceptibility, hazard, and risk. These landslides were retrieved from the work of Depicker et al. (2021) (<https://doi.org/10.5194/esurf-9-445-2021>).

Sampling strategy

We extracted all landslides from the inventory of Depicker et al. (2021) (<https://doi.org/10.5194/esurf-9-445-2021>) that occurred within our study area (confined by the extent of the panchromatic orthomosaic).

Data collection

A.D., B.S. processed the aerial photographs into an orthomosaic between 2018 and 2020. These photographs are conserved at the Royal Museum for Central Africa, Belgium. The landslide data were provided by Depicker et al. (2021) (<https://doi.org/10.5194/esurf-9-445-2021>). Between 2017 and 2020, A.D. collected the following datasets from literature and/or online repositories:

- the land cover data for 1988 and 2001, provided by Basnet and Vodacek, 2015 (<https://doi.org/10.3390/rs70606683>)
- the 2016 land cover data, provided by ESA (<http://2016africalandcover20m.esrin.esa.int/>)
- the Global Human Settlement Layer (GHSL), be accessed at <http://ghsl.jrc.ec.europa.eu/>
- the SRTM digital elevation model, provided by the USGS (<https://earthexplorer.usgs.gov/>)
- the seismic data (PGA), provided by Delvaux et al. (2017) (<http://dx.doi.org/10.1016/j.jafrearsci.2016.10.004>)
- The road data, downloaded from OpenStreetMap (<https://www.openstreetmap.org/#map=7/50.510/4.475>)
- the lithology data, retrieved from the work of Depicker et al. (2020) (<https://doi.org/10.1016/j.geomorph.2019.106886>) and can be requested from the author.

Timing and spatial scale	The data for this work were collected from 2017 to 2020. We sampled data for our study area which covers roughly 21,000 square kilometer.
Data exclusions	We excluded areas of young lithology from our analysis because we do not fully understand forest-landslide interactions in this context (https://doi.org/10.5194/esurf-9-445-2021).
Reproducibility	We provide all datasets necessary to reproduce this work. The new data that we present here (the 1958 forest) can be accessed at https://doi.org/10.5281/zenodo.5027117 . The landslide data can be downloaded at https://doi.org/10.5281/zenodo.5027004 . The custom Python script can be requested from the authors.
Randomization	Randomization was applied to estimate the uncertainty of the landslide susceptibility model. In order to obtain the 80% confidence interval, we trained the model 200 times, each time using 4,367 landslide instances that were sampled (with replacement) from the inventory of Depicker et al. (2021). In order to estimate the quality of the susceptibility model, we applied cross-validation. We calculated the model 10 times, each time creating a random training sample (90% of the data) and a validation sample (the other 10% of the data).
Blinding	Blinding was not used due to the nature of our samples (landslides, which are mechanical processes).
Did the study involve field work?	<input type="checkbox"/> Yes <input checked="" type="checkbox"/> No

Reporting for specific materials, systems and methods

We require information from authors about some types of materials, experimental systems and methods used in many studies. Here, indicate whether each material, system or method listed is relevant to your study. If you are not sure if a list item applies to your research, read the appropriate section before selecting a response.

Materials & experimental systems

Methods

- | n/a | Involvement in the study |
|-------------------------------------|--|
| <input checked="" type="checkbox"/> | <input type="checkbox"/> Antibodies |
| <input checked="" type="checkbox"/> | <input type="checkbox"/> Eukaryotic cell lines |
| <input checked="" type="checkbox"/> | <input type="checkbox"/> Palaeontology and archaeology |
| <input checked="" type="checkbox"/> | <input type="checkbox"/> Animals and other organisms |
| <input checked="" type="checkbox"/> | <input type="checkbox"/> Human research participants |
| <input checked="" type="checkbox"/> | <input type="checkbox"/> Clinical data |
| <input checked="" type="checkbox"/> | <input type="checkbox"/> Dual use research of concern |

- | n/a | Involvement in the study |
|-------------------------------------|---|
| <input checked="" type="checkbox"/> | <input type="checkbox"/> ChIP-seq |
| <input checked="" type="checkbox"/> | <input type="checkbox"/> Flow cytometry |
| <input checked="" type="checkbox"/> | <input type="checkbox"/> MRI-based neuroimaging |